SJ PH

A Novel Inexpensive, Rapid, Simple, and Sensitive Aptamer-Based Sandwich Assay for Colorimetric Thrombin Biosensing

Jack Andraka*, Noor Siddiqui*, Sheetal Ramsurran

Abstract

In this paper, we report the development of an aptamer-based colorimetric assay for the inexpensive, rapid, simple, and sensitive detection and quantification of biomolecules based on the principle of sandwich ELISA. Thrombin was selected as a model analyte to validate the assay design, which involved the selective binding of one or two different protein epitopes with DNA aptamers. Two different substrates were employed: covalently modified cellulose and glass microscope slides, with the covalently modified cellulose immobilizing the target analyte via non-specific divinyl sulfone (DVS) chemistry while the glass microscope slide strategy utilized a physisorbed thrombin aptamer as a capture agent. The captured biomolecules were then labeled by iron oxide nanoparticle-aptamer conjugates, which was then visualized via the reduction of Cu2+ ions onto the surface of the nanoparticles. An electrophoresis mobility shift assay and agarose gel electrophoresis were used to confirm the aptamer-thrombin binding and aptamer-nanoparticle conjugation, respectively. The formation of the copper film on the iron oxide nanoparticles was then modeled via a nucleation-catalytic growth model in order to optimize the assay run time. Both sensor formats had a high sensitivity with the cellulose-based assay having an limit of detection (LOD) of 50 pM whereas the glass-based assay demonstrated a higher sensitivity with an LOD of 20 pM. In addition, the sensors demonstrated high specificity to thrombin with no significant signal being elicited from exposure to Bovine-Serum Albumin (BSA). The cellulose-based assay had a material cost of $0.10 and took 15 minutes to run, representing a 60 times improvement in cost and a 16 times improvement in time when compared to the gold-standard for protein detection, ELISA. Thus, the developed assay represents an inexpensive, rapid, simple, sensitive, and versatile method for the detection of biomolecules for a host of applications from diagnostics to biodefense.

Introduction

The detection of biomolecules (proteins, DNA, RNA) provides valuable information for a broad array of applications including clinical diagnostics, environmental analysis, food safety, and biodefense [Wang et al. 2013]. However, current methods for the detection of proteins rely heavily on antibody-based immunoassays such as ELISA, Western blot, and lateral flow and generally require timely sample processing, expensive and complicated laboratory equipment, and highly trained technicians [Shafiee et al 2015]. As a result, the global health and biomedical communities have identified an urgent need for inexpensive, rapid, simple, and sensitive diagnostics for use in developing countries where the burden of infectious disease is highest.

Aptamers are single stranded oligonucleotides that selectively bind to various molecular targets, such as small molecules, proteins, nucleic acids, cells, or microorganisms [Song et al 2012]. Aptamers have a multitude of advantages over other biorecognition agents in bioassays due to their low cost, reproducibility, ease of isolation, reversible denaturing, good stability, and easy modification at virtually any desired site without loss of activity [Zhou et al 2014]. A variety of aptamer-based protein detection strategies have been described over the past few years, with approaches including fluorescence [Li et al 2014], electrochemistry [Jo et al 2015], inductively coupled plasma mass spectrometry [Ahn et al 2010], surface plasmon resonance [Cennamo et al 2015], and piezoelectrics [Neves et al 2015], yielding variable limits of detection, ranging from nanomolar to picomolar. However, many of these assays suffer from the same obstacles as their antibody counterparts, with test requiring timely sample processing, expensive and complicated laboratory equipment, and highly trained technicians, making these approaches ill-suited for resource-limited settings. In order to obviate

these difficulties, an aptamer-based biosensor was developed that combined the advantages of specific and sensitive detection of analytes found in immunoassays with the low cost and simplicity of optical readouts. The proposed assay utilizes either divinyl sulfone (DVS)-activated cellulose or aptamers physisorbed to glass microscope slides to immobilize a target biomolecule onto a solid substrate. The biomolecule is then labeled using aptamer-iron oxide nanoparticle conjugates and subsequently visualized by the reduction of Cu2+ ions onto the nanoparticles, which produces a visible color change that can be read by the naked eye or digital camera/cell phone camera.

As a proof of concept, thrombin, a serine protease involved in the last step of the coagulation cascade [Fenton et al 1981; Shuman et al 1986], was selected as a target molecule to assess the sensitivity and specificity of the developed assay. Thrombin is characterized by two distinct exosites, one binding fibrinogen (fibrinogen binding domain FBD) and the other binding heparin (heparin binding domain HBD) [Fenton et al 1981]. Two aptamers with high sensitivity and selectivity have been utilized for thrombin detection: TBA1, a 15-base pair DNA aptamer able to bind FBD and TBA2, a 29-base pair DNA aptamer able to recognize HBD [Meneghello et al 2012]. The concentration of thrombin in blood varies considerably: it can be almost absent in the blood of healthy subjects but can reach low-micromolar concentrations during the coagulation process [Shulman et al 1976]. In addition to its direct actions on the coagulation system, thrombin also functions as a potent signaling molecule that regulates physiologic and pathogenic responses. Thus, the developed biosensor for thrombin detection has potential for important clinical diagnostics as well as applications spanning from biodefense to environmental monitoring by altering the immobilization and detection aptamers.

Materials and Methods

Chemicals and Supplies

Unless otherwise stated, all chemicals were of analytical grade and obtained from Sigma Chemical Co. (St. Louis, MO). The sequence of the unmodified 15-mer TBA1 aptamer was: 5′-GGT TGG TGT GGT TGG-3′ and had a 5′-biotin modification to enable the conjugation of TBA1 aptamer to streptavidin coated iron oxide nanoparticles. The sequence of the unmodified 29-mer TBA2 aptamer was 5′-AGT CCG TGG TAG GGC AGG TTG GGG TGA CT-3′. All aptamers were synthesized by Thermo Fisher Scientific Co. (Waltham, Massachusetts), aliquoted to 10 µM, and stored at 4°C in TE buffer (10 mM Tris-HCl, 1mM EDTA) at a pH of 8.0. Human α-thrombin was purchased from Sigma Aldrich (St. Louis, MO) and dissolved in deionized water, aliquoted, and stored as recommended by the supplier. Streptavidin coated iron oxide nanoparticles were purchased from Nanocs Inc (Boston, Massachusetts) and stored at 4°C in 1x PBS (phosphate-buffered saline).

Electrophoresis Mobility Shift Assay Analysis for Binary Complexes

The binding of the two aptamers to the target analyte in solution was analyzed by an electrophoresis mobility shift assay (EMSA). Prior to incubation with thrombin, all aptamer samples (10 µM of oligonucleotide in a 100mM solution of KCl) were slow annealed by denaturing at 95°C and left to cool to room temperature. The folded aptamers were then diluted to 1 nM in TE buffer and then incubated with increasing concentrations (from 0 to 50 nM) of human thrombin in a total volume of 20 µL, at 25°C for 30 min. After incubation, the solutions containing free aptamer and thrombin-aptamer binary complexes were resolved by 12% non-denaturing polyacrylamide gels containing 1x TBE buffer (Tris-HCl 89 mM, borate 89 mM, EDTA 2 mM) and KCl 10 mM. The results of the assay were visualized with the fluorescent DNA binding dye Sybr Green II (Thermo Fisher Scientific), which preferentially binds to single-stranded DNA and emits fluorescence (excitement wavelength 488 nm, emission wavelength 522 nm) when bound to DNA. The fluorescence in the gels was detected via a Geliance 600 Imaging System (PerkinElmer).

Electrophoresis Mobility Supershift Assay Analysis for Ternary Complexes

To confirm the binding of the TBA1 and TBA2 aptamers to two distinct epitopes on thrombin to form an aptamer sandwich, a Supershift assay was utilized.

Both pairs of slow annealed aptamers (each 1 nM) were incubated simultaneously with the protein (5 nM) in a custom made binding buffer (Tris 20 mM, KCl 5 mM, NaCl 140 nM, MgCl2 1 mM, pH 7.5) in a total volume of 20µL, at 25°C for 30 min. Additionally, solutions of TBA1-thrombin and TBA2-thrombin binary complexes were prepared as described above. After incubation, solutions of free aptamers, binary complexes, and ternary complexes were also resolved by 12% non-denaturing polyacrylamide gels containing 1x TBE buffer (Tris-HCl 89 mM, borate 89 mM, EDTA 2 mM) and KCl 10 mM. The results of the assay were visualized with the fluorescent DNA binding dye Sybr Green II (Thermo Fisher Scientific), which preferentially binds to single-stranded DNA and emits fluorescence (excitement wavelength 488 nm, emission wavelength 522 nm) when bound to DNA. The fluorescence in the gels was detected via a Geliance 600 Imaging System (PerkinElmer).

Conjugation of Aptamers to Iron Oxide Nanoparticles and Confirmation via Agarose Gel Electrophoresis

TBA1 aptamers were purchased with a 5'-biotin modification and then conjugated to streptavidin coated iron oxide nanoparticles via biotin-streptavidin binding chemistry. To do this 100µL of TBA1 aptamers at a concentration of 1 µM was mixed with 100µL of 2 µg/mL of iron oxide nanoparticles and incubated at room temperature for 30 minutes. Unreacted aptamer was removed using centrifugal filtration five times at 3,000 rpm ( ). Gel electrophoresis was then carried out on 2% agarose gels with four samples: a 50 base-pair ladder, free TBA1 aptamer, aptamer-nanoparticle conjugates, and non-functionalized nanoparticles. The samples were then incubated in SYBR SAFE solution for 20 minutes and visualized under UV illumination (262 nm) by a Gel Doc XR+ Imaging System (BioRad). Zeta potential and particle size were calculated using dynamic light scattering (DLS) spectrophotometry (Zetasizer ZSP) at 25°C. Latex nanoparticles were used for calibration.

Preparation of Cellulose- and Glass-based Biosensors

DVS Activation of Cellulose

Physical adsorption is the simplest strategy for biomolecule immobilization onto solid substrates, with the immobilization of proteins onto supports such as polyvinlidene difluoride and nitrocellulose being well documented [Towbin et al 1979; Bode et al 1984; Tovey et al 1989]. However, these two substrates are limited in their ability to bind certain classes of biomolecules and are generally deficient towards the capture of nucleic acids, carbohydrates, and other small molecules, which limits their applicability in several important applications.

To alleviate this issue chromatography paper was activated with divinyl sulfone (DVS), which would non-specifically immobilize biomolecules form a sample onto the cellulose (see Figure 1). This approach would reduce the material cost and complexity of the assay but would sacrifice some sensitivity and specificity due to the non-specific immobilization strategy.

A 10% DVS (v/v, 0.1 M sodium carbonate, pH 11) solution was used to activate cellulose membranes chemically. Chr 1. Chromotography paper (Whatman, 12.0 x 9.0 cm2 sheets) were immersed in 20 mL of 10% DVS solution and incubated in separate 400-mL-capacity plastic zip lock bags and agitated for 2 hours on a rocking shaker. The activated cellulose was then removed from the bags, rinsed three times in a plastic tray with 100 mL of deionized water, and then dried for 2 hours under ambient conditions. The activated cellulose could be stored by placing in aluminum foil under ambient conditions to shield them from light and dust.

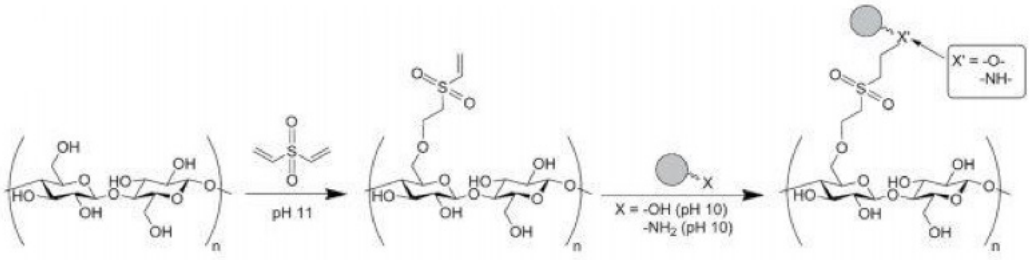

Figure 1. DVS Activation of Cellulose
Chemical Activation and functionalization of cellulose with biomolecules (gray) using DVS

Physisorption of TBA2 to Glass Microscope Slides

The glass microscope slide assay employed physisorbed TBA2 aptamer to immobilize human thrombin to the surface, which was then labeled using the aptamer-iron oxide nanoparticles. This approach increased the sensitivity and specificity of the assay due to the specific immobilization strategy but suffered from an increased material cost and complexity of creating the assay. Direct physisorption of the aptamers to the surface worked well with the concentration for physisorption being 15 µg/mL. 200 µL of the aptamer solution was pipetted directly onto the glass slide and after physisorption of the aptamers for 1 hour in a humid chamber at room temperature, each detection zone was washed with 1 x PBS and then the entire slide was washed with deionized water. The biosensors were then either run immediately or stored in a dry chamber at 4°C.

Colorimetric Sandwich Aptamer Assays

Serial dilutions of human thrombin were created in deionized water at concentrations between 1 pM and 1µM. These samples were then used to create calibration curves for the biosensors to determine their limit of detection (LOD). Additionally, a sample of 10 µM BSA was used to assess the specificity of the assay.

Cellulose-Based Assay

The cellulose-based assay was run by first directly pipetting 20 µL of the sample onto the DVS-activated cellulose and incubating for 3 minutes in a sterile petri dish at room temperature. Following this exposure, the paper was dipped in a 2% milk solution (obtained using dehydrated milk reconstituted with deionized water) and incubated in a sterile petri dish at room temperature for 2 minutes in order to block the membrane from reacting with the aptamer-iron oxide nanoparticle conjugates. After this the cellulose was washed three times with 1xPBS solution and then incubated with 20 µL of 1 µg/mL of the aptamer-iron oxide nanoparticle conjugate solution for 5 minutes in a sterile petri dish at room temperature. The cellulose was then washed three times with 1xPBS solution and 20 µL of 1 mM CuSO4 solution was pipetted onto the detection zone and incubated for 5 minutes in a sterile petri dish at room temperature in order to visualize the assay results.

Glass-Based Assay

The cellulose-based assay was run by first directly pipetting 20 µL of the sample onto the aptamer functionalized detection zone and incubating for 5 minutes in a sterile petri dish at room temperature. After this the slides were washed three times with 1xPBS solution and then incubated with 20 µL of 1 µg/mL of the aptamer-iron oxide nanoparticle conjugate solution for 5 minutes in a sterile petri dish at room temperature. The slides were then washed three times with

1xPBS solution and 20 µL of 1 mM CuSO4 solution was pipetted onto the detection zone and incubated for 5 minutes in a sterile petri dish at room temperature in order to visualize the assay results.

Data acquisition and processing

A digital camera with manual exposure settings (Nikon D1X) and a 1W white-light lamp (RadioShack) were attached to a stand so that they were the same distance away from the biosensors for each picture taken (see Figure 2) to ensure that all pictures have the exact same exposure so that measurements can be compared across assays. The measurement room was kept as dark as possible to prevent interference by room light, which could impact the exposure. All photographs were taken with a lens aperture of f5.6, a film speed of ISO 400, and a one second exposure time. The white-light lamp was warmed up for five minutes prior to taking a measurement and the assays were placed such that the entire substrate was in the camera's field of view. The sensors were photographed before and after copper reduction to set a baseline measurement to compare the end results to in order to establish absolute colorimetric change.

The photographs were then analyzed using the histogram tool in the blue-channel to quantitatively measure the color change and the final absorbance (A) was calculated according to the equation: $A = -\log(I)$, where I is the measurement prior to copper reduction while I is the measurement after copper reduction.

Modeling of Copper Film Formation

The extent of copper reduction under a range of surface iron oxide density and copper development time was predicted in order to minimize total assay time To guide model development (creating

a general mechanism and determining best-fit values of kinetic parameters – rate constants), a simplified experimental system of physisorbing different

Figure 2. Digital photography of assays. Setup for digital photography of assays. The camera and white light lamp were attached to a stand to ensure a constant distance from the substrate.

amounts of capture aptamers on the glass slide was used to produce a spectrum of surface iron oxide densities. This was achieved by adding varying concentrations of BSA as a competitor for physisorption on the glass microscope slide, with functionalization of a detection zone with a particular ratio of aptamers to BSA being done using an adapted procedure from Wild 2001. All tests were run as described previously with a thrombin concentration of 10 nM; however, colorimetric readings of the detection zone were taken every second during copper reduction to generate absorbance curves over time.

Results and Discussion

Thrombin Recognition by Biotin-Modified TBA1 and TBA2

EMSA Analysis of Binary Complexes

The results show that starting from a 2:1 ratio of thrombin to aptamer, the band of free aptamer gradually disappears as thrombin concentration increases while the band with greater molecular weight (lower mobility), corresponding to the TBA1-thrombin binary complex simultaneously appears (Figure 3, left). Thus, the results indicate that the biotin modification does not significantly impair the TBA1 thrombin binding. A similar assay was conducted with the TBA2 aptamer to confirm TBA2-thrombin binding. However, it appeared that the TBA2 aptamer was less sensitive than reported in the literature, implying potential error in the slow annealing for this aptamer or a faulty product (unlikely). Starting from a 10:1 ratio of thrombin to aptamer, the band of free aptamer also gradually disappears as thrombin concentration increases while the band of TBA2-thrombin binary complexes appears (Figure 3, right). An additional lane of 100 nM of thrombin was run for this binding interaction in order to better visualize the binding trend. Additionally, a decreased intensity of fluorescence signal for the TBA2 aptamer may also indicate a lower binding affinity between the indicator dye and the aptamer.

EMSA Analysis of Ternary Complexes

The results of the experiment indicate that the thrombin incubated with both aptamers was super-shifted, exhibiting a lower electrophoretic mobility than the binary complex, which is consistent with the formation of the ternary complex.

Confirmation of Aptamer-Iron Oxide Nanoparticle Conjugates

Conjugation of the 5'-biotin modified TBA1 aptamer with streptavidin coated iron oxide nanoparticles,

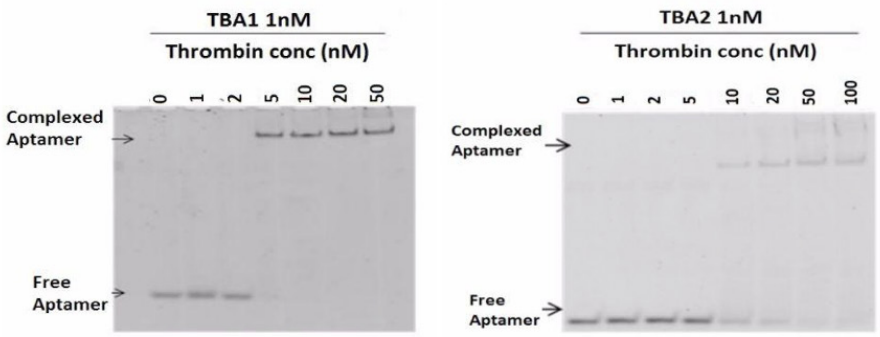

Figure 3. EMSA of Binary Complexes EMSA of TBA1-biotin with thrombin (left) and TBA2 with thrombin (right). TBA1 and TBA2 were separately incubated with the protein under the conditions described. The aptamer and thrombin concentrations are indicated as are the positions of the free aptamer and the binary complexes. A control reaction without thrombin was performed in all experiments. Binding reactions were resolved on a 12% non-denaturing PAA gel containing 1xTBE buffer and 10mM of KCl.

via biotin-streptavidin binding, successfully yielded aptamer-nanoparticle conjugates and led to an increase in both size (25.8±1.3 to 29.4±1.7 nm) and zeta-potential (-32.0±1.6 to -39.1±2.6 mV) of the nanoparticles. The conjugation of the TBA1 aptamer to the iron oxide nanoparticles was confirmed using agarose gel electrophoresis (Figure 5) with the free TBA1 aptamer matching the 15-bp band in the 50-bp ladder, and the aptamer-nanoparticle conjugate lane showing a band at a much higher molecular weight, confirming the conjugation of the aptamers to the nanoparticles. In addition, the spin filter purification successfully removed the free, unreacted aptamer from solution, thus preventing the potential reaction of free aptamers with bound thrombin.

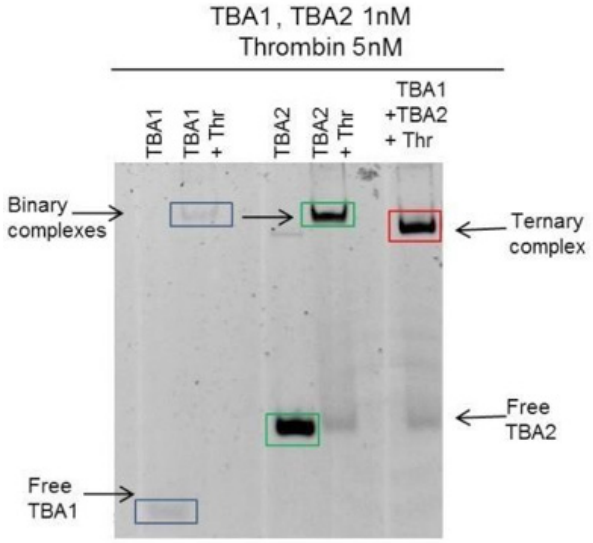

Figure 4. Supershift Assay of Ternary Complexes Electrophoretic Mobility Supershift Assay (EMSA) of 5'biotin-TBA1 +thrombin+TBA2. Each aptamer was incubated separately or simultaneously with thrombin under the conditions described. The aptamer and thrombin concentrations are indicated as are the free aptamer, binary complexes, and ternary complex bands. A reaction control without thrombin was performed for each aptamer. Binding reactions were resolved on a 12% PAA gel containing 1xTBE buffer and 10mM of KCl.

Modeling of Copper Film Formation

The kinetics of copper reduction onto the iron oxide nanoparticles revealed a sigmoid-shaped response (Figure 6c), with the presence of an induction period, followed by the rapid growth of colorimetric signal and termination of signal growth. For curve fitting, a variation of the four parameter equation was used:

$$A = A_{min} + \frac{A_{max} - A_{min}}{1 + e^{a*(t_{A,mid} - t)}}$$

Where A, A_{min}, A_{max} are the absorbance, minimum, and maximum values respectively, t is the time of copper reduction and tA, mid is the time at the point of inflection, and a is a curvature parameter (Figure 6a). Curve fitting was performed using GraphPad Prism 6 software for nonlinear regressions. R-squared values for best-fit curves were 0.92 (aptamer only), 0.99 (1:1 aptamer:BSA), 0.99 (1:2), 0.96 (1:4), 0.96 (1:8), and 0.71 (BSA only).

The copper reduction onto the iron oxide nanoparticles is believed to start with the catalytic formation of in situ copper nanoclusters [Sia et al 2004; Masnadi et al 2015] around iron oxide nanoparticles and undergo a general mechanism involving a nucleation step [Widegren et al 2003; Nyugen et al 2014] followed by an autocatalytic surface-growth step [Besson et al 2005; Watzky et al 1997]. It was also predicted that the mech-

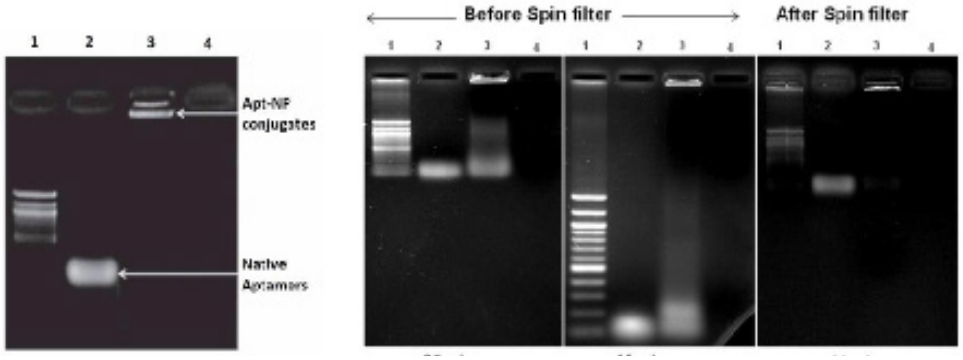

Figure 5. Confirmation of Aptamer-Iron Nanoparticle Conjugation Gel electrophoresis results of the aptamer-nanoparticle conjugates before and after spin filter purification. Lanes 1,2, 3, and 4 represent the 50 base-pair ladder, TBA1 aptamer, aptamer-nanoparticle conjugates, and unmodified nanoparticles, respectively.

anism for signal growth termination was reduced copper deposition due to agglomeration of nanoclusters to catalytically-inactive bulk metallic copper.

$$Cu\,(II) \rightarrow Cu(0) \quad k_1 \quad nucleation$$

$$Cu(II) + Cu(0) \rightarrow 2Cu(0) \quad k_2 \quad autocatalytic\ growth$$

The model focused on the first five minutes of copper reduction as during this period a sufficient signal is generated and both the nucleation and autocatalytic growth steps are present (Figure 6c). The model assumes irreversible reactions, fast adsorption of reactants onto the iron oxide surface, even distribution of iron oxide density across the detection zone, and negligible copper precipitate desorption. Based on these two reaction mechanisms, the following equation was created for copper reduction:

$$\frac{d}{dt}[Cu(0)] = k_1 S_{Fe}[Cu(II)] + k_2[Cu(II)][Cu(0)]$$

With the k1 being the rate constant of nucleation, k_2 being the rate constant of autocatalytic growth, and S_{Fe} being the surface density of iron oxide (expressed in moles of iron oxide nanoparticles per square meter of substrate). As the reaction progresses the number of active catalytic sites on the nanoparticles decrease due to the attachment of copper precipitate to the nanoparticles. As a result, SFe is expressed as a function of initial iron oxide surface density bound (S_{Fe}, I) and the extent of the nucleation reaction, δ:

$$S_{Fe} = S_{Fe,I}(1 - \delta)$$

To estimate S_{Fe}, I, the model assumed equal rates of physisorption between aptamer and BSA, a surface density of 0.5 µg/cm2 of aptamer for aptamer-only experimental conditions [Wild 2001], a 1:1 capture ratio of thrombin to physisorbed TBA2, and a 1:1 labeling ratio of thrombin to TBA1-nanoparticle conjugate. To relate the amount of captured thrombin with S_{Fe}, I, an averageiron oxide nanoparticle diameter of 25.8 nm was used (obtained from DLS measurements):

$$S_{Fe,I} = f_{Apt} * 3.3 \times 10^{-8}$$

Where f_{apt} is the percentage of aptamer to BSA in the physisorption solution.To estimate δ, a time tn was defined beyond which negligible copper reduction occurs from nucleation on iron nanoparticles (since all surfaces of nanoparticles are already covered by reduced copper). This time was calculated by finding the intersection between the lines tangent to the best-fit curve of reduced copper formation at tA, mid and t = 0 (Figure 6a). The active catalytic surface area was then expressed as

$$S_{Fe,I} = f_{Apt} * 3.3 \times 10^{-8}$$

The dependence of t_n on iron oxide nanoparticle density immobilized on the sensor surface by the aptamer sandwich interaction is shown in Figure 3b, and this relationship is generalized by an exponential decay fit:

$$S_{Fe} = S_{Fe,I}\left(1 - \frac{t}{t_n}\right)$$

Where $t_{n,\,max}$, $t_{n,\,min}$, are t_n at aptamer only and 1:8 aptamer to BSA surface coverage with k as a curvature parameter. The R-squared value of this fit was 0.97.

The developed model was then improved by comparing model predictions with the experimental data obtained for five different iron oxide concentrations. The two rate constants were determined via minimization of model error, which was performed using the pattern search algorithm (Direct search toolbox, Matlab) since this method handles the constrained nonlinear optimization problems in a short timeframe and does not require the function to be differentiable and continuous. By minimizing the objective function, the nucleation rate constant (k_1) and the autocatalytic growth rate constant (k_2) were determined to be $10^{-6} s^{-1}$ and 20 $m^3 mol^{-1} s^{-1}$, respectively (m^3 appears in the second rate constant due to the use of density measurements). To determine the goodness of fit between the model and the experimental results, the objective function was normalized by the total integral of the experimental curves over the five iron oxide concentrations (Figure 6d). The difference between the models predictions and the experimental results was found to be 9.2%.

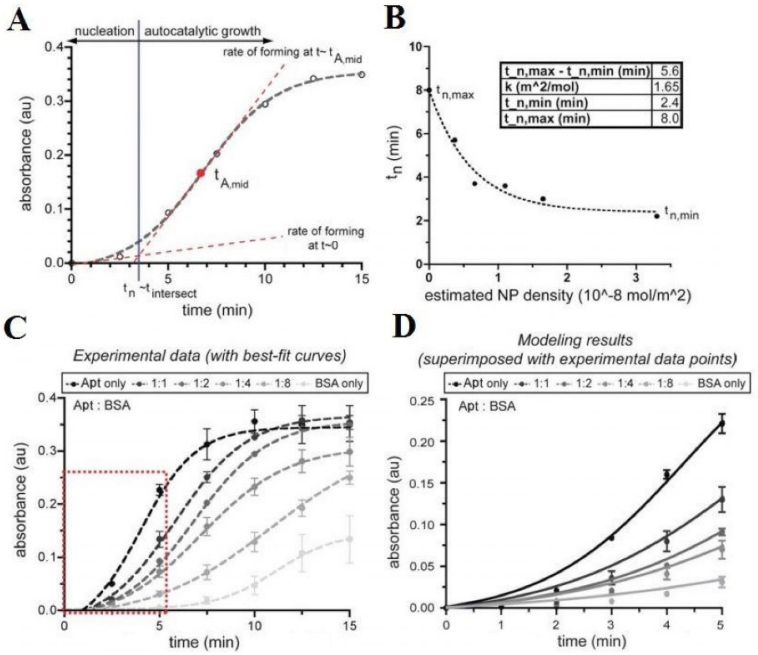

Figure 6. Modeling of Copper Reduction Modeling of copper reduction. (a) Copper reduction on detection zone with a 1:2 aptamer to BSA physisorption ratio. Data points are mean absorbance values, and the dashed line is the best-fit curve (four parameter logistic equation. (b) Dependence of tn on iron oxide nanoparticle density captured on the surface, with best-fit curve (exponential decay) as dashed line and best-fit parameters listed in the adjacent table. (c) Experimental kinetic data of copper reduction for various aptamer to BSA physisorption ratios. Data points indicate mean values, error bars indicate one standard deviation. Dashed lines are best-fit curves. (d) Computational modeling results (solid lines) superimposed with experimental data points. The difference (expressed as a normalized objective function) between the model and experiment was 9.2%

Development of Colorimetric Sandwich Aptamer Assay for Thrombin

The aptamer-coated glass microscope slides and DVS-activated cellulose were employed as solid substrates for the immobilization of thrombin as well as the formation of the aptamer sandwich for the colorimetric detection of thrombin. A thrombin calibration curve was constructed for both assay formats using serial dilutions of thrombin in deionized water and measuring the resulting color change using a digital camera in conjunction with Adobe Photoshop. Overall, the analytical capacity of both sensors for the detection of thrombin exceeded expectations with limits of detection of 10 pM (glass-based assay) and 20pM (cellulose-based assay), while demonstrating a wide detection range (10pM-200nM for glass and 20pM-1µM for cellulose). Additionally, the glass-based assay demonstrated no response in the presence of 1xBSA as a negative control and the activated cellulose assay demonstrated a very small response (absorbance of 0.07 au at a concentration of 10 µM). The difference in the responses of the two assay formats is hypothesized to be caused by the non-specific vs specific immobilization of thrombin onto the substrate. Additionally, both calibration curves had excellent R2 values of 0.97 and 0.98 for the best-fit curves for the cellulose-based assay and the glass-based assay, respectively. The signal between different concentrations eventually became indistinguishable due to the saturation phenomena where all captured aptamers became bound.

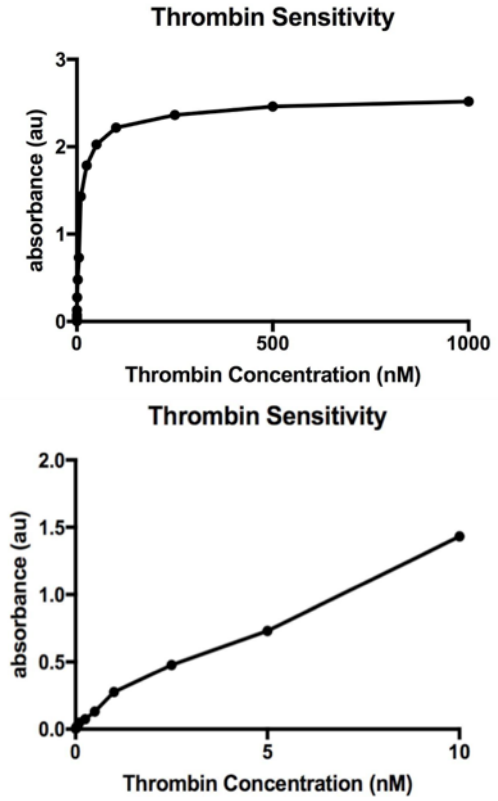

Figure 7. Thrombin Calibration Curves Calibration curves for thrombin for the glass-based assay. Serial dilutions of thrombin were prepared in deionized water with concentrations ranging between 1 pM and 1 µM. It was found that there was a strong linear response (R2 = 0.99) in the most clinically relevant range of 100 pM to 10 nM; however, after 50 nM the saturation phenomena caused the sensor response to plateau.

Conclusions

In order to meet the urgent demand for a method for the inexpensive, rapid, simple, sensitive, and specific a novel aptamer sandwich assay was developed. The assay consisted of a aptamers physisorbed to a glass microscope slide or DVS-activated cellulose for the immobilization of the target analyte along with a labeling solution of aptamer-iron oxide nanoparticle conjugates and a developing solution of Cu2+. Both sensor formats were highly sensitive with LODs of 10 pM (glass-based) and 20 pM (cellulose-based). When compared to traditional ELISA the sensor has a shorter detection time by a magnitude of 16 times (15 minutes vs 4 hours) and is 60 times less expensive ($0.10 vs $6.00). Future work will focus on incorporating the assay into a microfluidic cassette as well as developing a compact reader to simplify assay operation, multiplexing multiple detection zones onto a single device to detect multiple analytes, further optimizing analytical parameters (catalyst-reduction pair, pH, etc.) to increase sensitivity. It is believed that the developed assays could be a powerful method for the inexpensive, rapid, simple, sensitive, and selective detection of biomolecules for applications ranging from clinical diagnostics and biodefense to environmental monitoring and food safety.

Acknowledgements

We would like to thank Dr. Pease for advising us throughout the process and providing us the lab space for the physisorption and conjugation experiments as well as the Quake lab for providing

us lab space for the EMSA assays, agarose gel assay, and biosensing/modeling experiments. Additionally, we would like to thank Dr. Provine and Dr. Howe for advising us throughout our experiments. We would also like to acknowledge Ryan Cohen for aiding us in editing our Matlab scripts and helping to develop the model of the copper reduction. We would also like to acknowledge the following papers for providing the inspiration and details for some of our experiments:

- EMSA/Supershift assay: Hellman et al. 2007; Electrophoretic mobility shift assays 2005; Sosic et al. 2013.
- Analysis of aptamer-nanoparticle conjugation: Leach et al 2016; Sperling et al 2010
- DVS-activation of cellulose: Yu et al 2012
- Modeling: formation of copper precipitate (Sia et al 2004; Masnadi et al 2015), copper nanoclusters (Widegren et al 2003; Nyugen et al 2014), autocatalytic surface-growth (Besson et al 2005; Watzky et al 1997), aptamer ratio tuning (Wild 2001)

References

Ahn, J., Lee, S. W., Kang, H. S., Jo, M., Lee, D., Laurell, T., & Kim, S. (2010). Aptamer Microarray Mediated Capture and Mass Spectrometry Identification of Biomarker in Serum Samples. J. Proteome Res. Journal of Proteome Research, 9(11), 5568-5573. doi:10.1021/pr100300t

Besson, C., Finney, E. E., & Finke, R. G. (2005). A Mechanism for Transition-Metal Nanoparticle Self-Assembly. J. Am. Chem. Soc. Journal of the American Chemical Society, 127(22), 8179-8184. doi:10.1021/ja0504439

Bode, L., Beutin, L., & Köhler, H. (1984). Nitrocellulose-enzyme-linked immunosorbent assay (NC-ELISA) — A sensitive technique for the rapid visual detection of both viral antigens and antibodies. Journal of Virological Methods, 8(1-2), 111-121.doi:10.1016/0166-0934(84)90045-4

Cennamo, N., Pesavento, M., Lunelli, L., Vanzetti, L., Pederzolli, C., Zeni, L., & Pasquardini, L. (2015). An easy way to realize SPR aptasensor: A multimode plastic optical fiber platform for cancer biomarkers detection. Talanta, 140, 88-95. doi:10.1016/j.talanta.2015.03.025

Electrophoretic mobility shift assays. (2005). Nature Methods Nat Meth, 2(7), 557-558. doi:10.1038/nmeth0705-557

Hellman, L. M., & Fried, M. G. (2007). Electrophoretic mobility shift assay (EMSA) for detecting protein–nucleic acid interactions. Nat Protoc Nature Protocols, 2(8),1849-1861. doi:10.1038/nprot.2007.249

Jo, H., Gu, H., Jeon, W., Youn, H., Her, J., Kim, S., . . . Ban, C. (2015). Electrochemical Aptasensor of Cardiac Troponin I for the Early Diagnosis of Acute Myocardial Infarction. Analytical Chemistry Anal. Chem., 87(19), 9869-9875. doi:10.1021/acs.analchem.5b02312

Leach, J., Wang, A., Ye, K., & Jin, S. (2016). A RNA-DNA Hybrid Aptamer for-Nanoparticle-Based Prostate Tumor Targeted Drug Delivery. IJMS International Journal of Molecular Sciences, 17(3), 380. doi:10.3390/ijms17030380

Li, X., Ma, K., Zhu, S., Yao, S., Liu, Z., Xu, B., . . . Tian, W. (2014). Fluorescent Aptasensor Based on Aggregation-Induced Emission Probe and Graphene Oxide. Analytical Chemistry Anal. Chem., 86(1), 298-303. doi:10.1021/ac403629t

Masnadi, M., Yao, N., Braidy, N., & Moores, A. (2015). Cu(II) Galvanic Reduction and Deposition onto Iron Nano- and Microparticles: Resulting Morphologies and Growth Mechanisms. Langmuir, 31(2), 789-798. doi:10.1021/la503598b

Meneghello, A., Sosic, A., Antognoli, A., Cretaio, E., & Gatto, B. (2012). Development and Optimization of a Thrombin Sandwich Aptamer Microarray. Microarrays, 1(3), 95-106. doi:10.3390/microarrays1020095

Neves, M. A., Blaszykowski, C., Bokhari, S., & Thompson, M. (2015). Ultra-high frequency piezoelectric aptasensor for the label-free detection of cocaine. Biosensors and Bioelectronics, 72, 383-392. doi:10.1016/j.bios.2015.05.038

Shafiee, H., Asghar, W., Inci, F., Yuksekkaya, M., Jahangir, M., Zhang, M. H., . . . Demirci, U. (2015). Paper and Flexible Substrates as Materials for Biosensing Platforms to Detect Multiple Biotargets. Sci. Rep. Scientific Reports, 5, 8719. doi:10.1038/srep08719

Sia, S. K., Linder, V., Parviz, B. A., Siegel, A., & Whitesides, G. M. (2004). An Integrated Approach to a Portable and Low-Cost Immunoassay for Resource-Poor Settings. Angewandte Chemie Angew. Chem., 116(4), 504-508. doi:10.1002/ange.200353016

Song, K., Lee, S., & Ban, C. (2012). Aptamers and Their Biological Applications. Sensors,12(12), 612-631. doi:10.3390/s120100612

Sosic, A., Meneghello, A., Antognoli, A., Cretaio, E., & Gatto, B. (2013). Development of a Multiplex Sandwich Aptamer Microarray for the Detection of VEGF165 and Thrombin. Sensors, 13(10), 13425-13438. doi:10.3390/s131013425

Sperling, R. A., & Parak, W. J. (2010). Surface modification, functionalization and bioconjugation of colloidal inorganic nanoparticles. Philosophical Transactions of the Royal Society A: Mathematical, Physical and Engineering Sciences, 368(1915),1333-1383. doi:10.1098/rsta.2009.0273

Thanh, N. T., Maclean, N., & Mahiddine, S. (2014). Mechanisms of Nucleation and Growth of Nanoparticles in Solution. Chemical Reviews Chem. Rev., 114(15), 7610-7630. doi:10.1021/cr400544s

Tovey, E. R., & Baldo, B. A. (1989). Protein binding to nitrocellulose, nylon and PVDF membranes in immunoassays and electroblotting. Journal of Biochemical and Biophysical Methods, 19(2-3), 169-183. doi:10.1016/0165-022x(89)90024-9

Towbin, H., Staehelin, T., & Gordon, J. (1979). Electrophoretic transfer of proteins from polyacrylamide gels to nitrocellulose sheets: Procedure and some applications. Proceedings of the National Academy of Sciences, 76(9), 4350-4354. doi:10.1073/pnas.76.9.4350

Wang, J., & Qu, X. (2013). Recent progress in nanosensors for sensitive detection of biomolecules. Nanoscale, 5(9), 3589. doi:10.1039/c3nr00084b

Watzky, M. A., & Finke, R. G. (1997). Transition Metal Nanocluster Formation Kinetic and Mechanistic Studies. A New Mechanism When Hydrogen Is the Reductant: Slow, Continuous Nucleation and Fast Autocatalytic Surface Growth. J. Am. Chem. Soc. Journal of the American Chemical Society, 119(43), 10382-10400. doi:10.1021/ja9705102

Widegren, J. A., & Finke, R. G. (2003). The Problem of Distinguishing True Homogeneous Catalysis from Soluble or Other Metal-Particle Heterogeneous Catalysis under Reducing Conditions. ChemInform, 34(39). doi:10.1002/chin.200339278

Wild, D. (2001). Separation systems. In The Immunoassay handbook (2nd ed., pp. 149-158).London: Nature Pub. Group.

Yu, A., Shang, J., Cheng, F., Paik, B. A., Kaplan, J. M., Andrade, R. B., & Ratner, D. M. (2012).

Biofunctional Paper via the Covalent Modification of Cellulose †. Langmuir, 28(30),11265-11273. doi:10.1021/la301661x

Zhou, W., Huang, P. J., Ding, J., & Liu, J. (2014). Aptamer-based biosensors for biomedical diagnostics. The Analyst Analyst, 139(11), 2627. doi:10.1039/c4an00132j